Earth Syst. Dynam. Discuss., 6, 2043–2062, 2015
www.earth-syst-dynam-discuss.net/6/2043/2015/
doi:10.5194/esdd-6-2043-2015

Earth System Dynamics Discussions
Open Access
EGU

A simple model of the anthropogenically forced CO_2 cycle

W. Weber[1,*,†], **H.-J. Lüdecke**[2,*], **and C. O. Weiss**[3,*]

[1]Technical University Dortmund, Institute of Physics, Dortmund, Germany
[2]HTW, University of Applied Sciences, Saarbrücken, Germany
[3]Physikalisch-Technische Bundesanstalt, Braunschweig, Germany
[*]retired
[†]deceased 2014

Received: 21 September 2015 – Accepted: 7 October 2015 – Published: 20 October 2015

Correspondence to: H.-J. Lüdecke (moluedecke@t-online.de)

Published by Copernicus Publications on behalf of the European Geosciences Union.

Abstract

From basic physical assumptions we derive a simple linear model of the global CO_2 cycle without free parameters. It yields excellent agreement with the observations reported by the carbon dioxide information analysis center (CDIAC) as time series of atmospheric CO_2 growth, of sinks in the ocean and of absorption by the biosphere. The agreement extends from the year 1850 until present (2013). Based on anthropogenic CO_2 emission scenarios until 2150, future atmospheric CO_2 concentrations are calculated. As the model shows, and depending on the emission scenario, the airborne fraction of CO_2 begins to decrease in the year $\sim$2050 and becomes negative at the latest in $\sim$2130. At the same time the concentration of the atmospheric CO_2 will reach a maximum between $\sim$500 and $\sim$900 ppm. As a consequence, increasing anthropogenic CO_2 emissions will make the ocean and the biosphere the main reservoirs of anthropogenic CO_2 in the long run. Latest in about 150 years, anthropogenic CO_2 emission will no longer increase the CO_2 content of the atmosphere.

1 Introduction

Before the beginning of the industrial time and considerable land use the ratio of CO_2 in the atmosphere and in the oceans had been stationary. At the beginning of the industrial era (AD $\sim$ 1750) the atmospheric CO_2 concentration was 277 ppm (Frank, 2010), corresponding to $2.12 \times 277 = 587$ Gt C with 2.12 Gt C ppm^{-1} as the ratio of atmospheric carbon to CO_2 concentration (Le Quere, 2015). The CO_2 content of the ocean is much higher, approximately 37 000 Gt C (Post, 1990).

Presently (2013), the atmospheric CO_2 concentration has risen to 395 ppm, or to an extra of $(395 - 277) \times 2.12 = 250$ Gt C, mainly due to fossil fuel burning, slash-and-burn of forests and cement production. The total anthropogenic CO_2 production is $\sim$ 10 Gt C yr^{-1} or $\sim$ 4.7 ppm yr^{-1} CO_2. About 2.5 ppm yr^{-1} of this quantity remains in the

ESDD
6, 2043–2062, 2015

atmosphere, the rest is absorbed by the ocean and the biosphere in roughly equal amounts (CDIAC, 2015).

Since 1959 observations and measurements of atmospheric CO_2 contents and fluxes between atmosphere, ocean and biosphere have increased substantially. The first stock of these data was established in the year 2006, the latest as "Global Carbon Budget 14" in the year 2014 (CDIAC, 2015). The latter covers the years from 1959–2013. The "Global Carbon Budget 14" is used in the present paper. Historic CO_2 data for the preceeding years 1850 until 1959 are also given by CDIAC (2015). However, no systematic comparison of the extensive CDIAC data with any CO_2 global circulation model has been published till now.

Modeling the carbon cycle under the forcing of anthropogenic CO_2 emissions has been published among others by Revelle and Suess (1957) and Oeschger (1975). Most model work before 1970 is cited by Oeschger (1975). In particular, Joos (2013) describes the details of the 15 best known complex carbon circulation models and compares their results on the response to a CO_2 impulse of 100 Gt C in the year 2010. Modern models include the details of complex interactions between atmosphere, ocean and biosphere with their pertinent parameters. Among these are saturation of the ocean uptake under increasing atmospheric CO_2 concentrations, soil respiration, mixed atmospheric and oceanic multi-layers, divisions of the hemispheres into segments, and more than one time constant for the CO_2 exchange of atmosphere, ocean, and biosphere. The model parameters are obtained from observations, measurements and fitting procedures. Oeschger (1975), for instance, extracts model parameters from ^{14}C concentration measurements.

The results of atmospheric $^{14}CO_2$ measurements (Levin, 2010), which showed the interruption of the natural $^{14}CO_2$ equilibrium by the nuclear bomb test program, yielded new insight in the CO_2 exchange between atmosphere and ocean. However, the rapid decrease of $^{14}CO_2$, of an initial thousandfold concentration compared to the natural level, after the end of the bomb tests, has caused some confusion between the residence time RT and the adjustment time AT of an artificial CO_2 excess in the atmo-

ESDD
6, 2043–2062, 2015

sphere. The RT of CO_2 has the rather small value of ~ 5 years, whereas the AT is more than an order of magnitude higher (RT and AT values in half-life). The carbon exchange between atmosphere and ocean of $\sim 90\ \mathrm{Gt\,C\,yr^{-1}}$ compared with the pertinent present carbon net flux of $\sim 2\ \mathrm{Gt\,C\,yr^{-1}}$ explains the difference (IPCC, 2013; Cawley, 2011). The abrupt end of the bomb tests left a fast decreasing $^{14}CO_2$ flux from atmosphere into the ocean without a counterpart of the opposite way. In contrast to this, the $^{12}CO_2$ fluxes are always in two directions and are similar in magnitude because the CO_2 partial pressures of the upper ocean layer and the atmosphere are nearly equal.

In contrast to complex CO_2 circulation models, our objective was to model the anthropogenic forced CO_2 cycle by a minimum of physical assumptions and approximations. Therefore, we use only a single time constant for the atmospheric-oceanic net flux of CO_2 and obtain the model parameters from measurements. The validity of the model results is verified by comparison with CDIAC (2015). As a model input we use the anthropogenic CO_2 emissions from 1850 until present. From the response to a hypothetical CO_2 impulse of 100 Gt C in the year 2010, as proposed and used by Joos (2013) for the comparison of the 15 circulation models mentioned above, we evaluate the CO_2 remaining from the impulse and compare it with the results of Joos (2013).

2 The model

In the following carbon quantities and fluxes instead of CO_2 quantities are preferentially used. The mentioned factor $2.12\ \mathrm{Gt\,C\,ppm^{-1}}$ (Le Quere, 2015) yields the conversion between both. For clarity, carbon fluxes [$\mathrm{Gt\,C\,yr^{-1}}$] are written in small and their integrated values [Gt C] in capital letters.

Our model makes only two assumptions: Firstly, the carbon net-flux between atmosphere and ocean $n_s(t)$ can be approximated by

$$n_s(t) = 1/\tau \cdot (N_a(t) - N_0) \quad (1)$$

ESDD
6, 2043–2062, 2015

with $N_a(t)$ the carbon content of the atmosphere in the year t, $N_0 = N_a(1750) = 587.2\,\mathrm{Gt\,C}$ the pertinent value in the year 1750, and τ the time factor of the process. 587.2 Gt C is equivalent to 277 ppm atmospheric CO_2 concentration in the year 1750 (Frank, 2010) due to $587.2 = 277 \times 2.12$.

In a second assumption, biospheric increase $n_b(t)$ far from saturation is estimated as proportional to the atmospheric carbon increase $n_a(t)$

$$n_b(t) = b \cdot n_a\,(t) \tag{2}$$

with $n_a\,(t) = \mathrm{d}N_a\,(t)/\mathrm{d}t$ the carbon flux into the atmosphere, $n_b(t) = \mathrm{d}N_b(t)/\mathrm{d}t$ the carbon flux into the biosphere, and b the parameter of the process. By the basic Eqs. (1, 2) the model is linear.

In the following, bars are used for measured quantities for distinction from model quantities. Together with the anthropogenic carbon emissions $\overline{n}_{tot}(t)$ and Eq. (2) the sum rule

$$\overline{n}_{tot}(t) = n_a\,(t) + n_b(t) + n_s(t) = (1+b) \cdot n_a\,(t) + n_s(t) \tag{3}$$

and the equivalent sum rule for the integrated quantities

$$\overline{N}_{tot}(t) = N_a\,(t) + N_b(t) + N_s(t) \tag{4}$$

hold. Equations (1)–(3) can be combined to

$$\frac{dN_a\,(t)}{dt} = \left[\overline{n}_{tot}(t) - n_s(t)\right]/(1+b) = \left[\overline{n}_{tot}(t) - 1/\tau\left(N_a\,(t) - \overline{N}_0\right)\right]/(1+b). \tag{5}$$

$N_a(t)$ in Eq. (1) has to be completed with a temperature term because the equilibrium between oceanic and atmospheric partial CO_2 pressures shifts slightly with sea temperature,

$$\overline{S}_a(t) = \mu \cdot 2.12 \cdot \overline{T}(t) = 15.9 \cdot \overline{T}(t). \tag{6}$$

ESDD
6, 2043–2062, 2015

$\overline{S}_a(T)$ [Gt C] is the amount of carbon released into the atmosphere or absorbed by the ocean caused by changing temperatures, $\overline{T}(t)$ [°C] the average Earth temperature (HadCRUT4, 2015) converted to an anomaly around the AD 1850 value, μ the CO_2 production coefficient given by Frank (2010) as $\mu = 7.5\,\mathrm{ppm}\,^{\circ}\mathrm{C}^{-1}$, and $2.12\,[\mathrm{Gt\,C\,ppm}^{-1}]$ the already mentioned ratio of atmospheric carbon to CO_2 concentration. This completes the first order differential Eq. (5) to

$$\frac{\mathrm{d}N_a(t)}{\mathrm{d}t} = \left[\overline{n}_{tot}(t) - n_s(t)\right]/(1+b) = \left[\overline{n}_{tot}(t) - 1/\tau\left(N_a(t) + \overline{S}_a(t) - \overline{N}_0\right)\right]/(1+b). \quad (7)$$

Equation (7) has two parameters, $1/\tau$ of Eq. (1) and b of Eq. (2). The next paragraph shows that both parameters can be evaluated from measurements. Thus, the model has no free parameters.

With $\overline{N}_a(t_0)$ as initial condition for $t = t_0$, the measured total anthropogenic carbon emissions $\overline{n}_{tot}(t)$, and the temperature term $\overline{S}_a(t)$ the differential equation Eq. (7) can be solved numerically, yielding $N_a(t)$. By the sum rule Eq. (3), the quantities $n_s(t)$ and $n_b(t)$ are determined from $n_a(t)$. Finally, by numerical integration of $n_s(t)$, and $n_b(t)$ the quantities $N_s(t)$, and $N_b(t)$ are obtained.

The model results can be directly compared with the observed quantities for the period 1959–2013 (CDIAC, 2015), such as the atmospheric carbon content $\overline{N}_a(t)$, the integrated oceanic uptake $\overline{N}_s(t)$, and the integrated uptake of the biosphere $\overline{N}_b(t)$.

3 Model input and parameters

The following measurements, observations and estimations of carbon fluxes, which cover the years 1959–2013 are given by CDIAC (2015) and Le Quere (2015) and references cited therein: fossil fuel burning and cement production $\overline{n}_{fuel}(t)$, land use change such as deforestation $\overline{n}_{landuse}(t)$, atmospheric accumulation $\overline{n}_a(t)$, ocean sink $\overline{n}_s(t)$, and transforming organic materials in the biosphere $\overline{n}_b(t)$. The latter was estimated

ESDD
6, 2043–2062, 2015

from the residual of the other budget terms such as $\overline{n}_b = (\overline{n}_{fuel} + \overline{n}_{landuse}) - \overline{n}_a - \overline{n}_s$. The total anthropogenic emissions are $\overline{n}_{tot}(t) = \overline{n}_{fuel}(t) + \overline{n}_{landuse}(t) = \overline{n}_a(t) + \overline{n}_b(t) + \overline{n}_s(t)$. The graphs of $\overline{n}_a(t)$, $\overline{n}_b(t)$, and $\overline{n}_s(t)$ are given in the upper right and in both lower panels of Fig. 3 in red.

Data on carbon emissions from fossil fuel burning, cement production, and land use change, such as deforestation, which extend back to 1850 are also available from CDIAC (2015). For the times before 1959 the uncertainties associated with land use are estimated between 40–100 % (Houghton, 2007; Grainger, 2008). Atmospheric CO_2 concentrations as global means are given by Frank (2010) reaching back until the year 1000 AD.

The fluxes $\overline{n}_a(t)$, $\overline{n}_s(t)$, $\overline{n}_b(t)$ and the integrated values $\overline{N}_a(t)$, from $t_1 = 1959$ to $t_2 = 2013$, together with $\overline{N}_0 = \overline{N}_a(1750) = 587\,\mathrm{Gt\,C}$ yield the model parameters $1/\tau$ and b of the Eqs. (1) and (2) as

$$1/\overline{\tau} = \frac{\sum_{t_1}^{t_2} \overline{n}_s(t)}{\sum_{t_1}^{t_2} (\overline{N}_a(t) - \overline{N}_0)} = 0.01223 \tag{8}$$

or $\overline{\tau} = 81.7$ years and

$$\overline{b} = \frac{\sum_{t_1}^{t_2} \overline{n}_b(t)}{\sum_{t_1}^{t_2} \overline{n}_a(t)} = 0.668. \tag{9}$$

Gloor (2010) used Eq. (1) for the oceanic CO_2 uptake as well and estimated $\overline{\tau}$ as 81.4 years in excellent agreement with the result of Eq. (8).

Future global anthropogenic emissions in $\mathrm{Gt\,C\,yr^{-1}}$ are estimated by Höök (2010) as six different scenarios which end in the year 2100 (Fig. 1). The extreme scenario A1FI has an integrated value of ~ 2000 Gt C. However, estimates for the coal reserves of the Earth cite numbers of ~ 1100 Gt C (WCA, 2015). Therefore, we assume as tentative

ESDD
6, 2043–2062, 2015

data for our model after AD 2100 until 2150 a decrease of anthropogenic carbon emissions. Because no estimates for this future period are available we assume arbitrarily for all six scenarios a linear decrease of $\overline{n}_{\mathrm{tot}}$ to half the value of the year 2100.

4 Solving the model equations

The integration of a first order differential equation $\mathrm{d}y/\mathrm{d}t = f(t, y(t))$ such as Eq. (7) can be simply carried out by the explicit EULER technique (Butcher, 2003).

$$y(t + \Delta t) = y(t) + \Delta t \cdot f(t, y(t)) \tag{10}$$

The use of more elaborate numerical methods, such as RUNGE-KUTTA, yields no substantially different results for Eq. (7). With a time step of $\Delta t = 1$ year and an initial value $\overline{N}_{\mathrm{a}}(t_0)$, Eqs. (7) and (10) lead to the following iteration (i = 1, 2, ...):

$$n_{\mathrm{a}}(t_i) = \frac{1}{1+b}\left[\overline{n}_{\mathrm{tot}}(t_{i-1}) - 1/\tau\left(N_{\mathrm{a}}(t_{i-1}) + \overline{S}_{\mathrm{a}}(t_{i-1}) - \overline{N}_0\right)\right] \tag{11}$$

$$N_{\mathrm{a}}(t_i) = N_{\mathrm{a}}(t_{i-1}) + n_{\mathrm{a}}(t_i) \cdot \Delta t \tag{12}$$

and further to

$$n_{\mathrm{s}}(t_i) = \overline{n}_{\mathrm{tot}}(t_i) - (1+b) \cdot n_{\mathrm{a}}(t_i) \tag{13}$$

$$n_{\mathrm{b}}(t_i) = \overline{n}_{\mathrm{tot}}(t_i) - n_{\mathrm{a}}(t_i) - n_{\mathrm{s}}(t_i) \tag{14}$$

$$N_{\mathrm{b}}(t_i) = N_{\mathrm{b}}(t_{i-1}) + n_{\mathrm{b}}(t_i) \cdot \Delta t \tag{15}$$

$$N_{\mathrm{s}}(t_i) = N_{\mathrm{s}}(t_{i-1}) + n_{\mathrm{s}}(t_i) \cdot \Delta t. \tag{16}$$

The airborne fraction $\mathrm{AF}(t) = n_{\mathrm{a}}(t)/\overline{n}_{\mathrm{tot}}(t)$ is obtained from the result $n_{\mathrm{a}}(t)$ of Eq. (11). Initial values of $\overline{N}_{\mathrm{s}}(t_0)$ and $\overline{N}_{\mathrm{b}}(t_0)$ are not known. Thus, the values are uncertain by an additive constant. Therefore, the starting values in the left upper panel of Fig. 3 are

ESDD
6, 2043–2062, 2015

arbitrary and shifted for clarity. For the early period 1850–1959 only $\overline{n}_{tot}(t)$, $\overline{n}_a(t)$ and $\overline{N}_a(t)$ are available from observations. For the period 1959–2013 these data and additionally $\overline{n}_a(t)$, $\overline{n}_s(t)$, and $\overline{n}_b(t)$ were measured. For the future 2013–2150 only scenarios of $\overline{n}_{tot}(t)$ can be used.

The root of the squared differences between the integrated quantities of observations $\overline{N}_a(t)$, $\overline{N}_s(t)$, $\overline{N}_b(t)$ and their pertinent model counterparts yields a measure of the model accordance with the observations, for the period 1850–1959 as

$$G = \sqrt{\sum_{t=1851}^{1959} \left[\overline{N}_a(t) - N_a(t)\right]^2} \tag{17}$$

and for the period 1959–2013 as

$$F = \sqrt{\sum_{t=1960}^{2013} \left[\overline{N}_a(t) - N_a(t)\right]^2 + \left[\overline{N}_s(t) - N_s(t)\right]^2 + \left[\overline{N}_b(t) - N_b(t)\right]^2}. \tag{18}$$

Due to the different data basis, the iteration equations Eqs. (11)–(16) are solved separately for the following periods: For 1851–1959 we apply Eqs. (11) and (12) and the initial value $\overline{N}_a(1850) = 605.8\,\mathrm{Gt\,C}$ which yields G of Eq. (17). For the period 1960–2150 we use Eqs. (11)–(16) and the initial value $\overline{N}_a(1959) = 670.85\,\mathrm{Gt\,C}$ which yields F of Eq.(18). For the future we use Eqs. (11) and (12), the initial value $\overline{N}_a(2013) = 838.1\,\mathrm{Gt\,C}$, and emission scenarios for $\overline{n}_{tot}$.

The model allows to evaluate the adjustment time AT of reestablishing a stationary state after a CO_2 perturbation. We followed Joos (2013) by applying a CO_2 impulse of 100 Gt C in the year 2010 and evaluated the model response as the time dependent CO_2 amount remaining from the impulse. As an alternative test, we assumed the anthropogenic CO_2 emission from 2013 on completely stopped and analyzed the decreasing atmospheric CO_2 from this time on. The results from both tests are compared below.

ESDD
6, 2043–2062, 2015

An alternative method of parameter optimization

In order to judge the reliability of the values $\overline{\tau}$, $\overline{b}$, determined from Eqs. (8) and (9), an independent second method is helpful. For this purpose, τ and b can be determined by nonlinear optimization. We restricted the iteration to the period 1959–2013 of the more reliable measurements. The procedure minimizes the objective function $F(\tau, b)$ given by Eq. (18). We note that we could also have used a related objective function of the fluxes, instead of the integrated fluxes, as direct data. However, the large scatter of the fluxes leads the minimization very often to local minima. In contrast, minimizing the objective function for the integrated fluxes always yields unique global minima. For the minimizing procedure we applied the SIMPLEX method of Nelder and Mead (1965) with randomly generated starting values.

5 Results

Table 1 gives the model results for the parameters $\overline{\tau}$, $\overline{b}$ from Eqs. (8) and (9) and for τ, b evaluated by nonlinear optimization. The results $F(\tau, b)$ and $G(\tau, b)$ from nonlinear optimization and F, G from measurements agree well. According to Table 1 also the temperature term does not play a substantial role. Figures 2–4 depict the time series of the observations against their model counterparts. These latter are obtained without the temperature term and with τ, b from nonlinear optimization. In corresponding figures that would use $\overline{\tau}$, $\overline{b}$ calculated with Eqs. (8) and (9) or include the temperature term, differences to the Figs. 2–4 can hardly be detected by eye.

Figure 2 shows the atmospheric CO_2, the anthropogenic CO_2 emissions $\overline{n}_{\mathrm{tot}}(t)$, and the airborne fraction $\mathrm{AF} = n_{\mathrm{a}}(t)/\overline{n}_{\mathrm{tot}}(t)$ from 1850 to 2013. Model and observation of the atmospheric CO_2 concentrations are hardly distinguishable by eye (upper panel). However, this agreement of integrated quantities does not occur for the airborne fraction since it is not an integrated quantity (lower panel).

ESDD
6, 2043–2062, 2015

Figure 3 shows the observations $\overline{N}_a(t)$, $\overline{N}_b(t)$, $\overline{N}_s(t)$, $\overline{n}_a(t)$, $\overline{n}_b(t)$, and $\overline{n}_s(t)$ from 1959 to 2013 together with their pertinent model time series. As already mentioned, $N_s(t)$ and $N_b(t)$ are uncertain by an additive constant and were shifted here for clarity.

Figure 4 covers the period 2013 until the future year 2150. The left panel shows the time series of atmospheric CO_2 caused by the six emission scenarios given by Höök (2010) and a CO_2 curve caused by a stop of anthropogenic CO_2 emissions in the year 2013. The right panel shows the airborne fractions caused by the six emission scenarios. All scenarios yield a maximum of the atmospheric CO_2, the earliest in the year ~ 2090, the latest in the year ~ 2130. At these times the airborne fraction changes sign. The steadily decreasing CO_2 in the left panel (magenta curve) is the result of the stop of anthropogenic CO_2 emissions at the year 2013. The CO_2 adjustment time AT evaluated from this event is $t_{1/2}$ = 103 years. At $t_{1/2}$ the carbon concentration reaches its half value $N_a(t_{1/2}) = [N_a(2013) - N_a(\infty)]/2$.

Figure 5 depicts the atmospheric CO_2 concentration and the response for a 100 Gt C impulse charged in the year 2010. After the year 2010 the anthropogenic carbon emissions are kept at the 2010 year-value of 10 Gt yr^{-1} as proposed by Joos (2013). The response function shows the percentage of carbon remaining from the impulse, obtained from the difference of the atmospheric carbon with and without the impulse and has an adjustment time AT of $t_{1/2}$ = 100 years. The upper panel shows that during the first 100 years after the impulse the decreasing CO_2 exceeds the upper limit of the far more comprehensive models, reported by Joos (2013). After the year 2200 the lower panel shows the model results distinctly below the range of the comprehensive models. In the long run the CO_2 concentrations of the model approach zero. The final difference of ~ 20 % is discussed below.

ESDD
6, 2043–2062, 2015

6 Summary and discussion

Our simple linear model gives excellent agreement with all relevant measurements, i.e. $\overline{N}_a(t)$, $\overline{N}_s(t)$, and $\overline{N}_b(t)$. Also the agreement with the rates $\overline{n}_a(t)$, $\overline{n}_s(t)$, and $\overline{n}_b(t)$ is on average excellent. That the fluctuations of the measured rates are larger than those of the model results is apparently due to the non-inclusion of natural variations (such as El Niño etc.). We mention as an important model result a decrease of the atmospheric CO_2 concentration from roughly 2100 on. We mention further that the change of the sea surface temperature since the beginning of industrialization had apparently no appreciable influence on the anthropogenically forced carbon cycle.

The perfect agreement of the linear model results with the measurements indicates, that we are far from influences of nonlinearities or the Revelle effect (Sabine, 2004; IPCC, 2013). An increase of the CO_2 content of the atmosphere by a factor of 2, as expected for the next 100 years, will therefore probably not cause substantial deviations from the linear model results. The model should therefore at least be suited for predictions during this nearer future period.

We note that on a decade to century scale the more elaborate models predict a faster decrease of the CO_2 concentration after the 100 Gt C test impulse than the linear model. On a century to millennium scale the more elaborate models predict a persistent CO_2 concentration, while the linear model shows a decrease to zero concentration with an adjustment time of 100 years.

The difference in the long run may stem from the Revelle effect, included in the elaborate models, a resistance to absorbing atmospheric CO_2 by the ocean due to bicarbonate chemistry. However, as Gloor (2010) underlines, there exists so far no evidence for the Revelle effect. Thus, such effects are presently hypothetical.

ESDD
6, 2043–2062, 2015

References

Butcher, J. C.: Numerical Methods for Ordinary Differential Equations, John Wiley and Sons, New York, USA, 2003. 2050

Cawley, G. C.: On the atmospheric residence time of anthropogenically sourced carbon dioxide, Energy Fuels, 25, 5503–5513, 2011. 2046

Carbon Budget 2014: Carbon Dioxide Information Analysis Center (CDIAC), Global Carbon Projct – Full Global Carbon Budget, Budget v1.1, available at: http://cdiac.ornl.gov (last access: June 2015), 2014. 2045, 2046, 2048, 2049

Frank, D. C., Esper, J., Raible, C. C., Büntgen, U., Trouet, V., Stocker, B., and Joos, F.: Ensemble reconstruction constraints on the global carbon cycle sensitivity to climate, Nature, 463, 527–532, historical CO_2 concentrations, available at: ftp://ftp.ncdc.noaa.gov/pub/data/paleo/contributions_by_author/frank2010/ (last access: June 2015), 2010. 2044, 2047, 2048, 2049

Gloor, M., Sarmiento, J. L., and Gruber, N.: What can be learned about carbon cycle climate feedbacks from the CO_2 airborne fraction?, Atmos. Chem. Phys., 10, 7739–7751, doi:10.5194/acp-10-7739-2010, 2010. 2049, 2054

Grainger, A.: Difficulties in tracking the long-term global trend in tropical forest area, P. Natl. Acad. Sci. USA, 105, 818–823, 2008. 2049

HADCRUT4, Climate Research Unit (GB), available at: www.cru.uea.ac.uk/cru/data/temperature/, last access: June 2015. 2048

Höök, M., Sivertsson, A., and Aleklett, K.: Validity of the fossil fuel production outlooks in the IPCC emission scenarios, Nat. Resour. Res., 19, 63–83, 2010. 2049, 2053, 2058, 2061

Houghton, R. A.: Balancing the global carbon budget, Ann. Rev. Earth Plan. Sc., 35, 313–347, 2007. 2049

IPCC Fifth Assessment Report, Chapter 6: Carbon and Other Biochemical Cycles, available at: http://www.ipcc.ch/report/ar5/wg1/ (last access: August 2015), 2013. 2046, 2054

Joos, F., Roth, R., Fuglestvedt, J. S., Peters, G. P., Enting, I. G., von Bloh, W., Brovkin, V., Burke, E. J., Eby, M., Edwards, N. R., Friedrich, T., Frölicher, T. L., Halloran, P. R., Holden, P. B., Jones, C., Kleinen, T., Mackenzie, F. T., Matsumoto, K., Meinshausen, M., Plattner, G.-K., Reisinger, A., Segschneider, J., Shaffer, G., Steinacher, M., Strassmann, K., Tanaka, K., Timmermann, A., and Weaver, A. J.: Carbon dioxide and climate impulse response functions for the computation of greenhouse gas metrics: a multi-model analysis,

ESDD
6, 2043–2062, 2015

Atmos. Chem. Phys., 13, 2793–2825, doi:10.5194/acp-13-2793-2013, 2013. 2045, 2046, 2051, 2053, 2062

Le Quéré, C., Moriarty, R., Andrew, R. M., Peters, G. P., Ciais, P., Friedlingstein, P., Jones, S. D., Sitch, S., Tans, P., Arneth, A., Boden, T. A., Bopp, L., Bozec, Y., Canadell, J. G., Chini, L. P., Chevallier, F., Cosca, C. E., Harris, I., Hoppema, M., Houghton, R. A., House, J. I., Jain, A. K., Johannessen, T., Kato, E., Keeling, R. F., Kitidis, V., Klein Goldewijk, K., Koven, C., Landa, C. S., Landschützer, P., Lenton, A., Lima, I. D., Marland, G., Mathis, J. T., Metzl, N., Nojiri, Y., Olsen, A., Ono, T., Peng, S., Peters, W., Pfeil, B., Poulter, B., Raupach, M. R., Regnier, P., Rödenbeck, C., Saito, S., Salisbury, J. E., Schuster, U., Schwinger, J., Séférian, R., Segschneider, J., Steinhoff, T., Stocker, B. D., Sutton, A. J., Takahashi, T., Tilbrook, B., van der Werf, G. R., Viovy, N., Wang, Y.-P., Wanninkhof, R., Wiltshire, A., and Zeng, N.: Global carbon budget 2014, Earth Syst. Sci. Data, 7, 47–85, doi:10.5194/essd-7-47-2015, 2015. 2044, 2046, 2048

Levin, I., Naegler, T., Kromer, B., Diehl, M., Francey, R. J., Gomez-Pelaez, A. J., Steele, L. P., Wagenbach, D., Weller, R., and Worthy, D. E.: Observations and modelling of the global distribution and long-term trend of atmospheric $^{14}CO_2$, Tellus B, 62, 26–46, 2010. 2045

Nelder, J. A., and Mead, R.: A simplex method for function minimization, Comput. J., 7, 308–313, 1965. 2052

Oeschger, H., Siegenthaler, U., Schotterer, U., and Gugelmann, A.: A box diffusion model to study the carbon dioxide exchange in nature, Tellus, XXVII, 168–192, 1975. 2045

Post, W. M., Peng, T.-H., Emanuel, W. R., King, A. W., Dale, V. H., and DeAngelis, D. L.: The global cycle, Am. Sci., 78, 310–326, 1990. 2044

Revelle, R., and Suess, H. E.: Carbon dioxide exchange between atmosphere and ocean and the question of an increase of atmospheric CO_2 during the past decades, Tellus, IX, 18–27, 1957. 2045

Sabine, C. L., Feely, R. A., Gruber, N., Key, R. M., Lee, K., Bullister, J. L., Wanninkhof, R., Wong, C. S., Wallace, D. W. R., Tilbrook, B., Millero, F. J., Peng, T.-H., Kozyr, A., Ono, T., and Rios, A. F.: The oceanic sink for anthropogenic CO_2, Science, 305, 367–371, 2004. 2054

WCA: World Coal Association, Coal Statistics (Reserves), available at: www.worldcoal.org/resources/coal-statistics/, last access: June 2015. 2049

ESDD
6, 2043–2062, 2015

Table 1. Results: $\overline{\tau}$ and $\overline{b}$ are extracted from Eqs. (8, 9), τ and b from nonlinear optimization; F, G, $F(\tau,b)$, $G(\tau,b)$ are the differences between model and measurements extracted from Eqs. (17, 18). Row 1 is with and Row 2 without the temperature term $\overline{S}_a(t)$ of Eq. (6).

$\overline{S}_a(t)$	$\overline{\tau}$ [yr]	$\overline{b}$	F	G	τ [yr]	b	$F(\tau,b)$	$G(\tau,b)$
$15.9 \cdot T(t)$	81.7	0.668	34.7	70.9	80.3	0.697	27.7	58.6
0	81.7	0.668	34.6	52.7	84.0	0.697	28.1	53.3

ESDD
6, 2043–2062, 2015

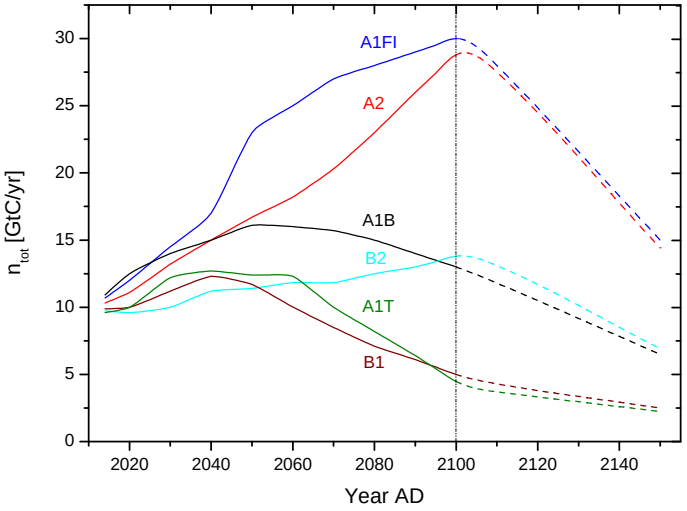

Figure 1. Future carbon emission scenarios until AD 2100 given by Höök (2010). Emissions from 2100 to 2150 are arbitrarily assumed to decrease linearly to half the 2100 year value.

ESDD
6, 2043–2062, 2015

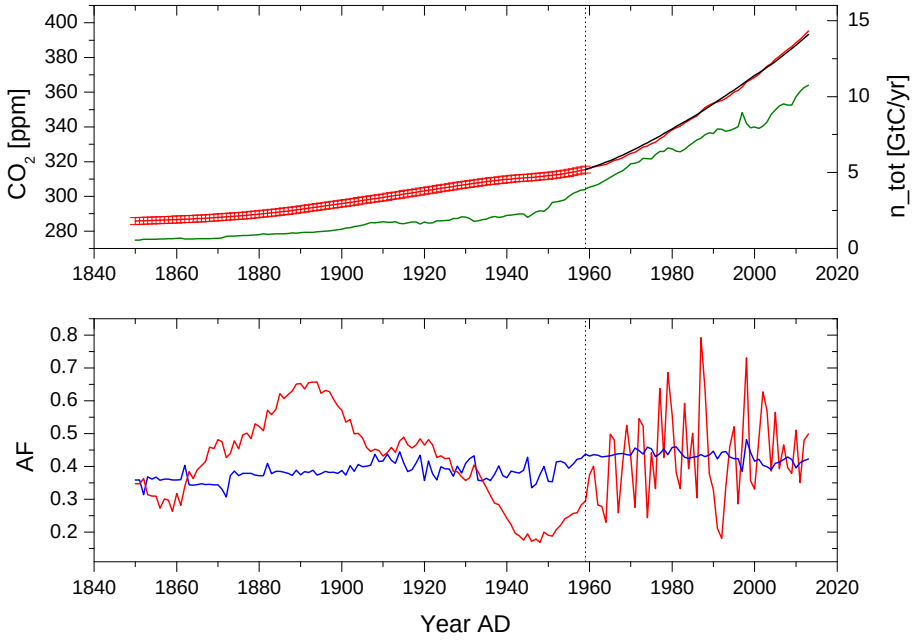

Figure 2. Results for the period 1850–2013. Upper panel, left y axis: model (black) and observations (red) of atmospheric CO_2 concentrations; in the period 1850 to 1959 the observation uncertainties are indicated. Upper panel, right y axis: Total anthropogenic emissions $\overline{n}_{\mathrm{tot}}(t)$ (green). Lower panel: Airborne fraction AF = $n_{\mathrm{a}}/\overline{n}_{\mathrm{tot}}$ (model in blue, observations in red).

ESDD
6, 2043–2062, 2015

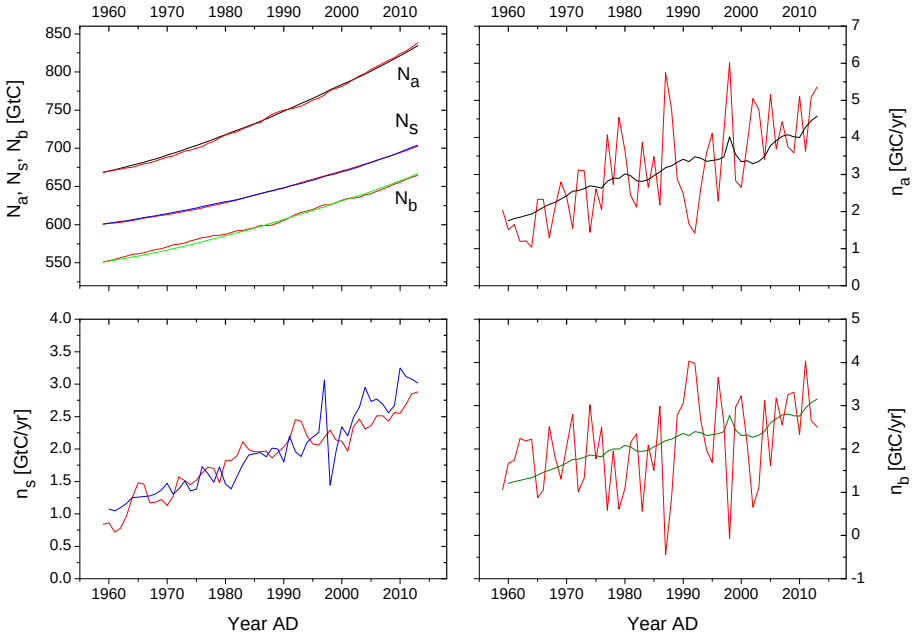

Figure 3. Results for the period 1959–2013. Model and observations of $N_a(t)$, $N_b(t)$, $N_s(t)$, $n_a(t)$, $n_b(t)$, and $n_s(t)$ (observations in red color). $N_b(t)$ and $N_s(t)$ in the left upper panel are shifted for clarity (N_a in the left upper panel identical except for the factor 2.12 with CO_2).

ESDD
6, 2043–2062, 2015

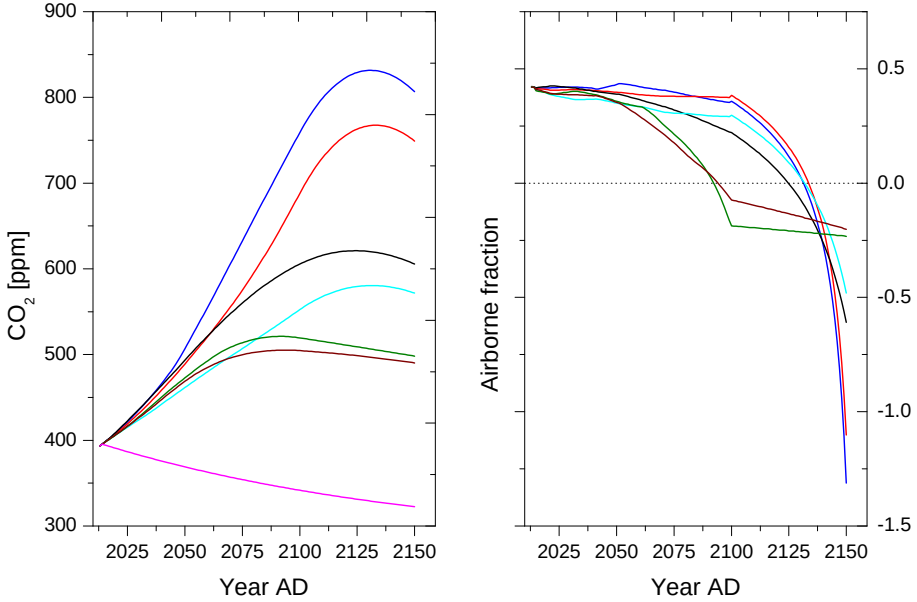

Figure 4. Results for the period 2013–2150. Left panel: Atmospheric CO_2 concentrations according to the scenarios given by Höök (2010), see Fig. 1: A1FI (blue), A2 (red), A1B (black), B2 (cyan), A1T (green), and B1 (brown). Zero emission of anthropogenic CO_2 from the year 2013 on causes the steadily decreasing magenta curve with an adjustment time $t_{1/2}$ of 103 years. Right panel: Airborne fraction AF = $n_a(t)/\overline{n}_{tot}(t)$ for the six emission scenarios. The horizontal dotted line indicates AF = 0 for clarity.

ESDD
6, 2043–2062, 2015

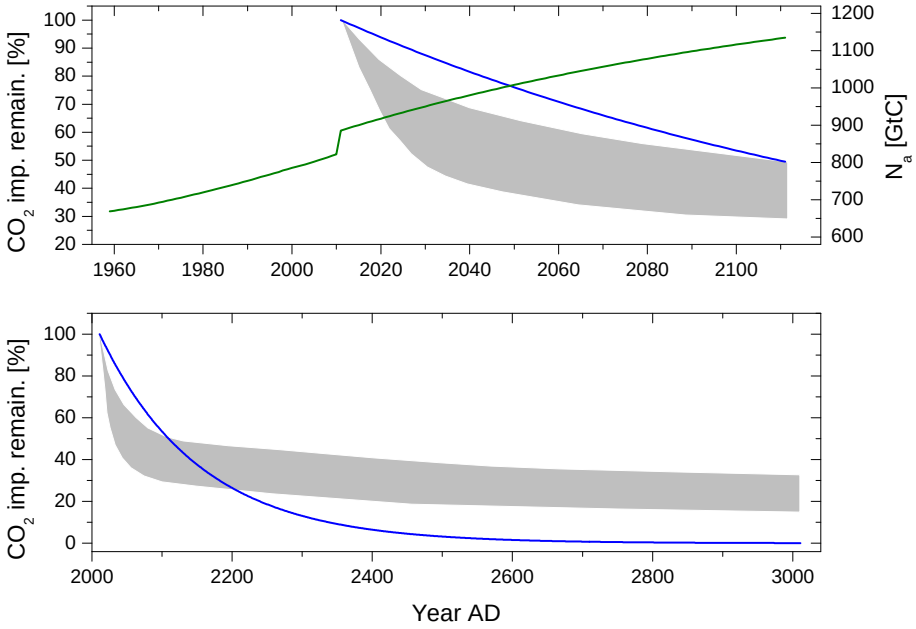

Figure 5. Results for the period 2013–3010. Upper panel, left y axis: CO_2 remaining from a 100 Gt C impulse in the year 2010 until the year 2110 (blue). Upper panel, right y axis: Atmospheric carbon content $N_a(t)$ (green). The impulse applied in 2010 is visible as a step in the green curve. Lower panel: CO_2 remaining as in the upper panel for a period of 1000 years. The adjustment time $t_{1/2}$ is 100 years. The grey shaded regions indicate the pertinent impulse responses of 15 models published by Joos (2013).

ESDD
6, 2043–2062, 2015